Topological phononic insulator with robust pseudospin-dependent transport

Bai-Zhan Xia,[1,*] Ting-Ting Liu,[1] Guo-Liang Huang,[2] Hong-Qing Dai,[1] Jun-Rui Jiao,[1] Xian-Guo Zang,[3] De-Jie Yu,[1] Sheng-Jie Zheng,[1] and Jian Liu[1]

[1]*State Key Laboratory of Advanced Design and Manufacturing for Vehicle Body, Hunan University, Changsha, Hunan 410082, People's Republic of China*

[2]*Department of Mechanical and Aerospace Engineering, University of Missouri, Columbia, Missouri 65211, USA*

[3]*College of Transportation & Logistics, Central South University of Forestry & Technology, Changsha, Hunan 410004, People's Republic of China*

(Received 15 February 2017; published 11 September 2017)

Topological phononic states, which facilitate unique acoustic transport around defects and disorders, have significantly revolutionized our scientific cognition of acoustic systems. Here, by introducing a zone folding mechanism, we realize the topological phase transition in a double Dirac cone of the rotatable triangular phononic crystal with C_{3v} symmetry. We then investigate the distinct topological edge states on two types of interfaces of our phononic insulators. The first one is a zigzag interface which simultaneously possesses a symmetric mode and an antisymmetric mode. Hybridization of the two modes leads to a robust pseudospin-dependent one-way propagation. The second one is a linear interface with a symmetric mode or an antisymmetric mode. The type of mode is dependent on the topological phase transition of the phononic insulators. Based on the rotatability of triangular phononic crystals, we consider several complicated contours defined by the topological zigzag interfaces. Along these contours, the acoustic waves can unimpededly transmit without backscattering. Our research develops a route for the exploration of the topological phenomena in experiments and provides an excellent framework for freely steering the acoustic backscattering-immune propagation within topological phononic structures.

DOI: 10.1103/PhysRevB.96.094106

I. INTRODUCTION

The intriguing discovery of a novel state of condensed matter, known as the topological order in the quantum spin Hall (QSH) effect system and the topological insulator [1–4], has inspired research for analogous states in bosonic systems, such as periodic photonic crystals [5–24]. External magnetic fields, which could break the time reversal (TR) symmetry of photonic systems, were initially utilized to realize topological orders of photons [6–10]. Dynamic modulation of system parameters has been successfully used to emulate effects of magnetic fields for desired topological properties [11,12,25–29]. Optical bianisotropic metamaterials, supporting strong spin-orbit interactions analogous to the QSH effects of the condensed matter systems, have also been developed [14–16,30,31].

Analogous to photons, phonons can also benefit from topologically robust states. Unfortunately, in airborne sound, the traditional spin-orbital interaction mechanism is invalid because of the inherent longitudinal nature of the acoustic polarization. Aiming at this issue, scientists have conducted abundant explorations. For gyroscopic mechanical systems, the phononic helical edge states against defects and disorders have been achieved in time-asymmetric gyroscopes emulating "magnetic fields" [32–35]. There are some studies on the modulated phononic crystals [36,37]. For fluid acoustic systems, the topologically protected edge modes have been theoretically realized in networks of acoustic cavities with circulating airflow [38–42], spatiotemporal modulation [43,44], or coupled resonators [45–47]. However, dynamic instability and inherent noise arising from the moving background are detrimental in their engineering applications.

The phononic honeycomb lattice with C_{6v} symmetry possesses an accident double Dirac cone with a fourfold degeneracy [48–53]. When the honeycomb lattice undergoes a symmetry inversion, the topological phase transition, inspired by the band inversion near the double Dirac cone, leads to a robust pseudospin-dependent one-way edge model [54,55]. Recently, Dirac and Dirac-like cones beyond the honeycomb lattice have been uncovered [47,56–61]. Furthermore, noncircular rods used to control the scattering and the band structure of sound have also been investigated [62]. Based on the group theory, the double Dirac cone cannot appear in artificial crystal lattices beyond C_{6v} symmetry [54,63]. Introducing a zone folding mechanism, Dirac cones at the K point in the Brillouin zone (BZ) of a honeycomb lattice folded to the double Dirac cone at the Γ point [21,55]. If we can further fold a double Dirac dispersion in a phononic crystal beyond the honeycomb lattice and experimentally observe the pseudospin-dependent one-way transport, the zone folding mechanism will break through the limitation of the point-group symmetry to mimic the pseudospin couplings. The phononic insulators in triangular lattices possess zigzag and linear interfaces. The distinct topological properties on these different interfaces, which have not been exploited, will develop our scientific cognition of the QSH effect of sound. Furthermore, the reconfigurability of the topological state, obtainable in condensed matter systems, is still absent in phononic systems. The well-reconfigurable synthetic acoustic media would offer great flexibility to manipulate the topologically protected sound transport.

*xiabz2013@hnu.edu.cn

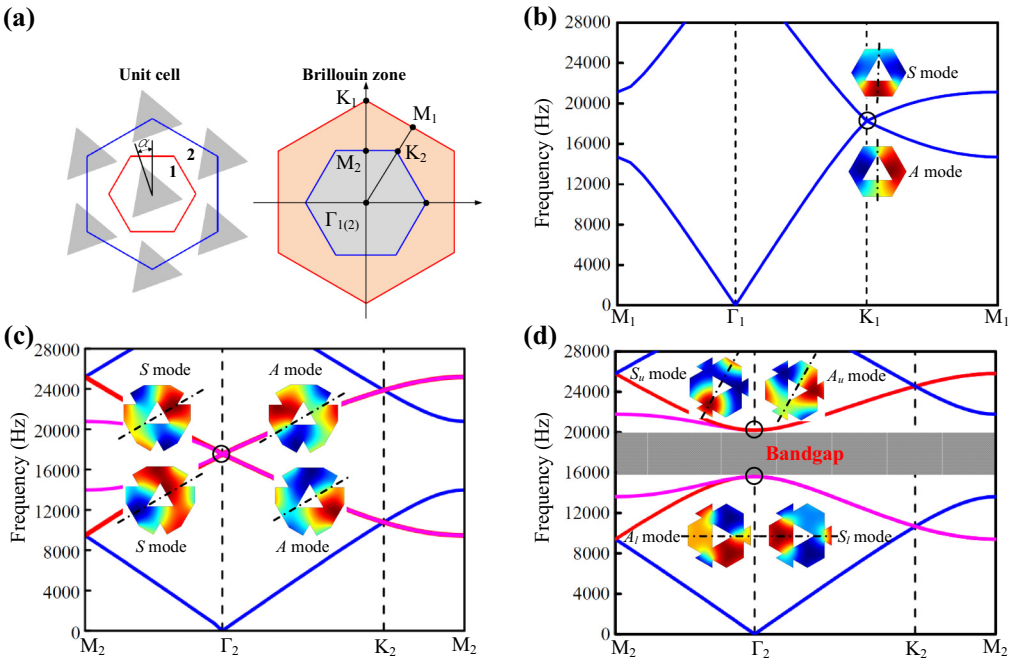

FIG. 1. Schematic of phononic crystal and its band structures. (a) Left panel: A geometric arrangement of phononic crystal consisting of rotatable triangular prisms with a lattice constant of 10 mm. The length of the triangular prism is 6.8 mm. Right panel: BZs of the primitive and larger hexagonal unit cells. (b) Band structure with a Dirac cone at the K point in the BZ of the primitive unit cell. (c) Band structure with a double Dirac cone at the Γ point in the BZ of the larger hexagonal unit cell. (d) Band structure with a complete band gap induced by rotating triangular prisms of 30°. Pressure field distributions at the Dirac and double Dirac cones are inserted in (b–d). Dashed lines are the symmetric axis. Numerical methods are presented in Method 1 of the Supplemental Material [65].

II. TUNABLE TOPOLOGICAL PHONONIC INSULATOR

Focusing on the above issues, we construct a phononic crystal formed with rotatable triangular prisms and illustrated in Fig. 1(a). The double Dirac cone, by increasing the degrees of freedom to twofold states, can efficiently mimic the analog of the pseudospin coupling and the QSH effect in a spin-1 acoustic system [54,55,64]. However, according to the point-group symmetry, the double Dirac cone is nonexistent in our phononic crystal with C_{3v} symmetry [54,63]. To break through this limitation, the zone folding mechanism [21,55] is employed. When taking a primitive hexagonal unit cell [marked by the blue line in Fig. 1(a)], this phononic crystal with C_{3v} symmetry carries Dirac dispersions at the K_1 points in the BZ [Fig. 1(b)]. When taking the larger hexagonal unit cell [marked by the red line in Fig. 1(a)], a double Dirac dispersion at the Γ_2 point is formed by folding four branches with Dirac dispersions (Fig. 1(c) and Note 1 of the Supplemental Material) [21,55,65]. The fourfold degeneracy at the double Dirac cone possesses two phononic modes, classed as the symmetric (S) mode and the antisymmetric (A) mode [inserted in Fig. 1(c)]. As Dirac cones are independent of the filling ratio [56], the degeneracy of the folded double Dirac cone cannot be lifted by tuning its filling ratio (Fig. S2 of Supplemental Material [65]). A viable alternative to lift the degeneracy of this double Dirac cone is breaking the mirrored symmetry [63]. The angular-dependent frequencies for the four band edges at the Γ_2 point are illustrated in Fig. S3 of the Supplemental Material [65]. Rotating the triangular prisms left or right by 30°, the phononic crystal yields the widest band gap at the original double Dirac cone (shown in Fig. S3 of Supplemental Material [65]). The complete band gap stems from the symmetry breaking because of the mismatch of the mirrored symmetries between the lattice and triangular prisms. The phononic crystal with a reduced inversion symmetry induces a pairwise coupling between the original Dirac bands [inserted in Fig. 1(d)]: the upper symmetric (S_u) mode and the lower antisymmetric (A_l) mode, as well as the upper antisymmetric (A_u) mode and the lower symmetric (S_l) mode. These symmetric and antisymmetric modes are perfectly identical with those in the phononic honeycomb lattice with C_{6v} symmetry [54]. For all frequencies in the proximity of the original double Dirac cone, these hybridized eigenmodes can efficiently emulate new pseudo-up-spin and pseudo-down-spin [21,31,54,55,64]. When the triangular prisms are rotated from left (or right) with an angle of 30° to right (or left) with an angle of 30°, a band inversion takes place (Figs. S3 and S4 of Supplemental Material [65]). This confirms a topological phase transition between triangular prisms with different rotational directions and provides a platform to configure the topological interface for robust one-way transport.

As shown in Fig. 2(a), we consider a triangular phononic lattice. There are two typical classes of interfaces across which the topological phases of phononic crystals are opposite. The first one is the zigzag interface along the x direction. The triangular prisms located at the top and bottom, respectively, rotate left and right by 30° [Fig. 2(b)]. Because of the topological phase transition, a pair of edge states respectively exhibiting S and A modes emerge within the overlapped bulk

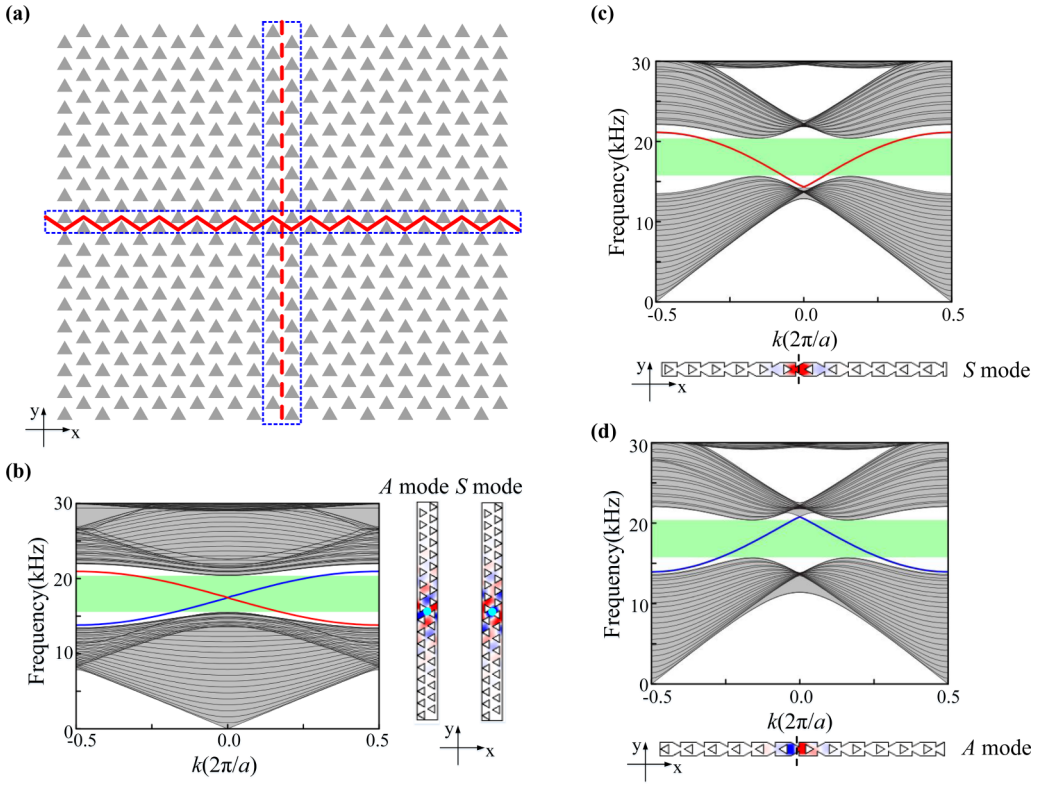

FIG. 2. Topological phononic insulator and its edge band structures. (a) A schematic of our topological phononic insulator with different interfaces along the x direction and the y direction. (b) Left panel: Band structure of a supercell consisting of 18×2 phononic crystals with a zigzag interface along the x direction. Right panel: Pressure field distributions of the supercell at $k = 0$. Edge modes of the blue and red lines are respectively symmetric and antisymmetric about the light blue node due to the point symmetry of the geometrical structure. (c) Top panel: Band structure of a supercell consisting of 12×2 phononic crystals (the left part turns left and the right part turns right) with a linear interface along the y direction. Bottom panel: The pressure field distribution of the supercell at $k = 0$. The edge mode is mirror symmetric about the dashed line. (d) Top panel: Band structure of a supercell consisting of 12×2 phononic crystals (the left part turns right and the right part turns left) with a linear interface along the y direction. Bottom panel: The pressure field distribution of the supercell at $k = 0$. The edge mode is antisymmetric about the dashed line. Gray lines are bulk bands. Pale green shaded regions are topological band gaps. Numerical methods are presented in Method 1 of the Supplemental Material [65].

band gap of two distinct phononic crystals [Fig. 2(b)]. These topological edge modes characterize the topological helical states, analogous to the unidirectional spin-polarized one-way propagation in condensed matter systems [21,31,54,55,64]. Therefore, although the mirrored symmetry breaking yields a band gap in which the acoustic propagation is efficiently prevented, the spins of edge states localized at the topological interface lead to a pseudospin-dependent one-way propagation. In this case, Gaussian beams can effectively transport through the zigzag interface (Fig. S5 of Supplemental Material [65]). Furthermore, when triangular prisms located at the top and bottom are switched, the same band structure and the same propagation phenomenon can be obtained (Fig. S6 of Supplemental Material [65]).

The other type of interface is a linear one along the y direction [shown in Fig. 2(a)]. When the triangular prisms located at the left and right sides of the linear interface respectively rotate left and right by 30°, a topological edge state with an S mode emerges [Fig. 2(c)]. However, when the triangular prisms located at the left and right sides of the linear interface are switched, a distinct topological edge state with an A mode appears [Fig. 2(d)]. Gaussian beams can effectively transmit through the linear interface with the S mode while blocking the case with the A mode (Fig. S7 of Supplemental Material [65]). The reason is that the locally symmetric edge state in each unit cell leads to robust propagation, while the locally antisymmetric one in each unit cell leads to a deep suppression of the edge mode (see Note 2 of Supplemental Material [65]). These findings reveal that the phononic crystals with different interfaces exhibit distinct topological edge states, which will greatly enhance our scientific cognition of topological insulators and provide an excellent platform for the realization of the distinct propagation characteristics of sound in an acoustic system.

III. PSEUDOSPIN-DEPENDENT EDGE MODE OF A TOPOLOGICAL PHONONIC INSULATOR

Here, we utilized a cross-waveguide splitter [30,54,66] to measure the pseudospin transport of our topological phononic insulator with a very high fidelity. As shown in Fig. 3(a), the splitter is divided into four sections with four input/output ports, marked as 1, 2, 3, and 4. In the top-left and bottom-right sections, triangular prisms are rotated left by 30°. In the

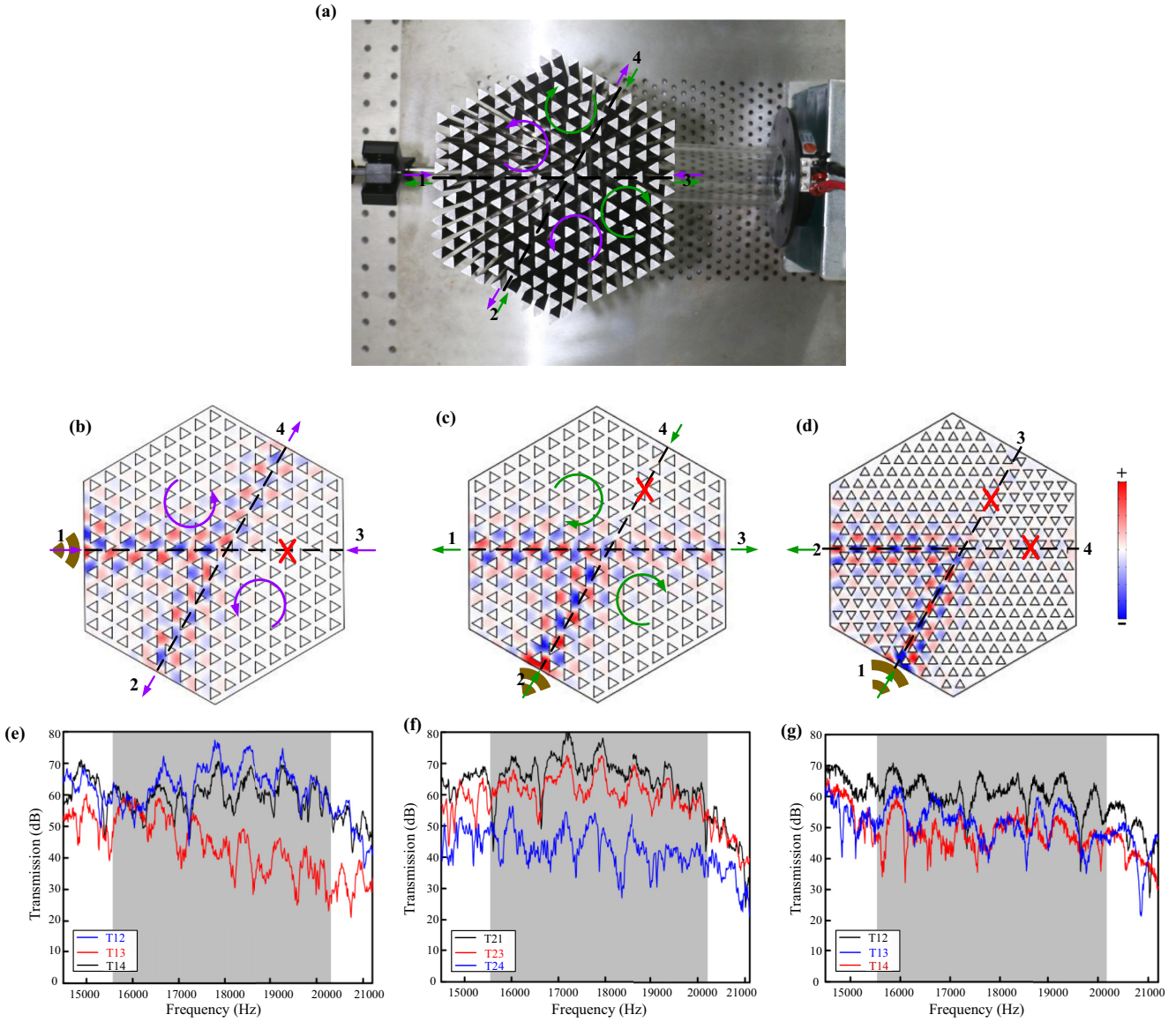

FIG. 3. Acoustic pseudospin-dependent edge mode at topological cross-waveguide splitter. (a) Photo of our topological cross-waveguide splitter. The anticlockwise (clockwise) edge circulating propagation is indicated by the purple (green) circular arrows. (b, c) Simulated acoustic pressure field for cases with zigzag interfaces at a frequency of 18.42 kHz. (d) Simulated acoustic pressure field for the case with linear interfaces at a frequency of 18.42 kHz. (e, f, g) Experimental transmission spectra for cases (b)–(d). T_{ij} indicates the transmission spectra from port i to port j ($i, j = 1, 2, 3, 4$). Shadow regions indicate topological band gaps. Experimental methods and measurements are presented in Method 2 of Supplemental Material [65].

top-right and bottom-left sections, triangular prisms are rotated right by 30°. The topological interfaces are zigzagged. When the acoustic wave propagates from port 1 (or port 3) to port 2 (or port 4) by crossing the junction, the triangular prisms rotated left and right are respectively located on the left and right sides of the paths. As the pseudospin-dependent state is determined by the spatial symmetry, the pseudospin-dependent edge states of the paths with the same spatial symmetries are always permitted. In this case, the acoustic wave from port 1 (or port 3) can propagate through the junction to port 2 and port 4 (labeled by purple lines). Similarly, the structural spatial symmetries of paths from port 2 (or port 4) to port 1 and port 3 are also preserved. However, for the path from port 1 to port 3, the rotation directions of the triangular prisms located on both sides are counterchanged when crossing the junction. Due to the inversion of the structural spatial symmetry, the pseudospin states are also inversed. These opposite pseudospin states cannot be excited by each other due to the mismatch of their spin configurations, indicating that the acoustic wave cannot propagate from port 1 to port 3. Similar results can be obtained for other straight paths (from port 3 to port 1, from port 2 to port 4, and from port 4 to port 2). Therefore, based on the opposite slope of the dispersion band, the individual spin edge state in Fig. 3(a), can only support a topological one-way propagation with an anticlockwise (purple circular arrows) or clockwise (green circular arrows) direction. This conclusion

is perfectly consistent with the simulation results illustrated in Figs. 3(b) and 3(c) and the experimental measurements presented in Figs. 3(e) and 3(f). However, this interesting acoustic counterpart of the QSH effect cannot emerge in the topological phononic insulators with linear interfaces [Figs. 3(d) and 3(g)], as their topological edge state exhibits only an *S* mode or an *A* mode, which inherently differ from the zigzag interfaces with both *S* and *A* modes. This is an essential condition to yield hybridized eigenmodes for pseudospin-dependent propagations [21,54,55]. This topological pseudospin behavior also vanishes in the nontopological structure (Fig. S8 of Supplemental Material [65]).

IV. TOPOLOGICALLY PROTECTED ACOUSTIC PROPAGATION AGAINST DEFECTS

To verify the robust transport property of our topological phononic insulator, two cases with different defects were intentionally introduced. The first one is an incomplete cross-waveguide splitter with several cavities (rounded by green circles). The other one is a cross-waveguide splitter with several disordered triangular prisms which inversely rotate (rounded by green circles). Cavities and disorders are not spin-mixing defects, indicating that the topological characteristics of our phononic insulator are not broken by these "nonmagnetic" impurities [9,54,64]. Simulated acoustic pressure fields, illustrated in Figs. 4(a) and 4(b), show that the acoustic waves from port 1 can effectively detour cavities and disorders, transmitting to ports 2 and 4. Experimental transmission spectra, plotted in Figs. 4(c) and 4(d), further verify the robustly pseudospin-dependent propagation of sound in the topological cross-waveguide splitter with "nonmagnetic" defects.

V. RECONFIGURABLE GUIDING OF THE TOPOLOGICAL EDGE MODE

Triangular prisms in our topological phononic insulator can freely rotate around their central axes. By rotating some triangular prisms in the left direction and the other ones in the right direction, arbitrarily sharpened contours between distinct phononic crystals can be created. To confirm this robust reconfigurable transport property, two nodes (A3 and A4) respectively located at the upper-right and bottom-left regions are selected. Figure 5(a) shows the acoustic wave from input port 1 effectively passing through nodes A3 and A4, finally reaching output port 2. Figure 5(c) shows the acoustic wave from input port 1 effectively passing through nodes A4 and A3, finally reaching output port 2. Compared with the transmission spectra of ordinary phononic crystals with gapped band structures, the transmission spectra measured for the above two configurations of topological phononic insulators exhibit a high transmission over the band-gap frequency range [Figs. 5(b) and 5(d)]. The other complicated pathways, including an asteroid pathway and an "HNU"-like pathway

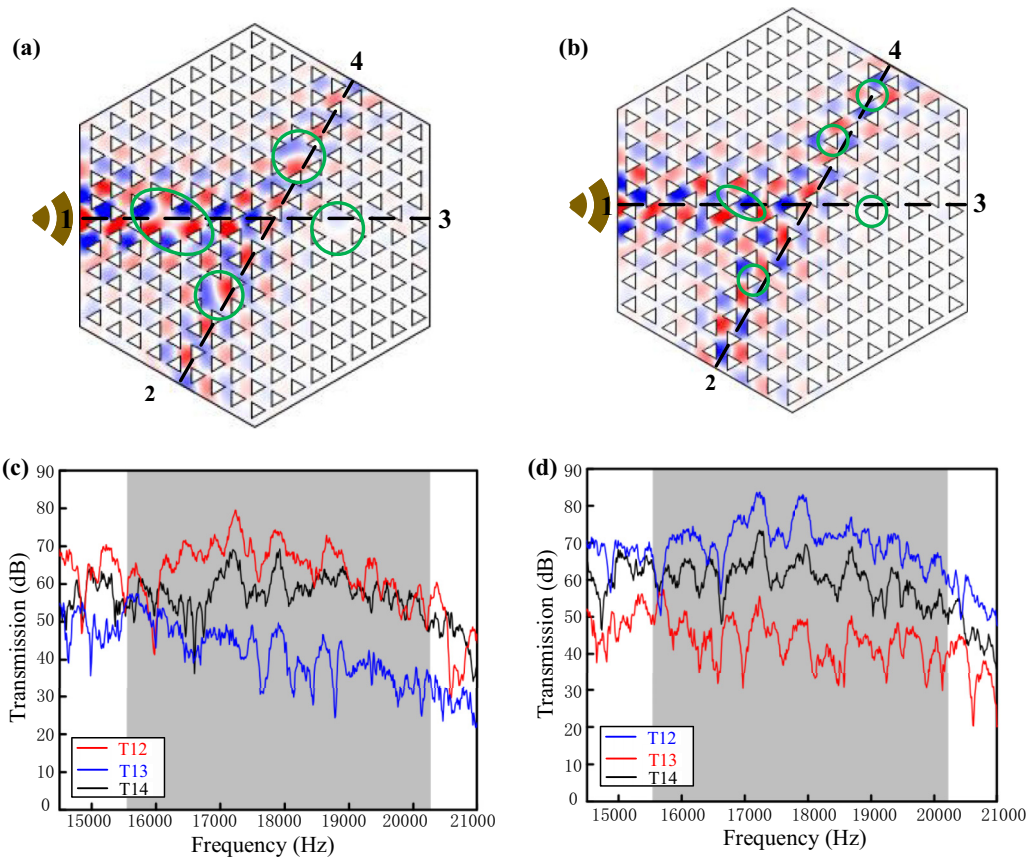

FIG. 4. Robust one-way transport. (a, b) Simulated acoustic pressure field at a frequency of 18.42 kHz in the topological phononic insulator with cavities and disorders. (c, d) Experimental transmission spectra. T12, T13, and T14 indicate the transmission spectra from port 1 to ports 2, 3, and 4. Shadow regions indicate topological band gaps.

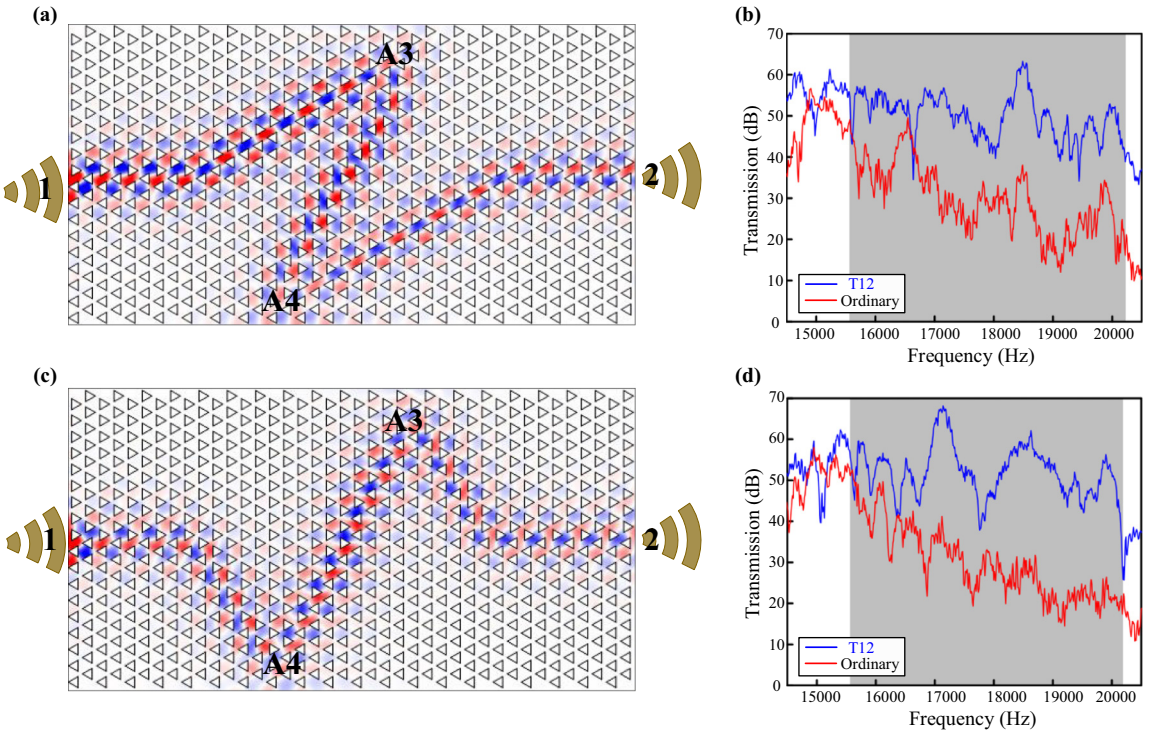

FIG. 5. Reconfigurable guiding of topological edge modes. (a, c) Simulated acoustic pressure field along the pathway through nodes A3 and A4. (c) Simulated acoustic pressure field distribution along the pathway through nodes A4 and A3. (b, d) Experimental transmission spectra for two pathways. The blue and red curves respectively indicate the transmission spectra in topological phononic insulators and ordinary phononic crystals. Shadow regions are topological band gaps.

which is the initials of Hunan University, are illustrated in Fig. S9 of the Supplemental Material [65]. This unparalleled ability to freely steer the robust topological propagation along arbitrary pathways opens an excellent avenue to design tunable topological acoustic devices.

VI. CONCLUSION

In conclusion, our topological platform experimentally verified the distinct topological properties related with zigzag and linear interfaces of phononic insulators and realized the fascinating phononic pseudospin phenomenon to "nonmagnetic" defects. In addition, the robust reconfigurable one-way edge state with controllable contour in our topological phononic insulator opens up infinite possibilities for manipulating and steering acoustic waves along arbitrary paths to any desired point without backscattering. Note that our reconfigurable topological phononic insulator can be easily extended to a broad acoustic spectrum, from audible sound to ultrasound, and even up to hypersound, by modulating its geometric parameters. More importantly, the intriguing topological phenomenon of our reconfigurable phononic insulator induced by a folded double Dirac conical dispersion in the phononic lattice with C_{3v} symmetry is a milestone in the design of modern topological phononic devices beyond C_{6v} symmetry and generates an impressive potential for applications in the foreseeable future.

ACKNOWLEDGMENTS

This work is supported by the National Natural Science Foundation of China (Grants No. 11402083 and No. 11572121), the National Key Research and Development Program of China (Grant No. 2016YFD0701105), and the Collaborative Innovation Center of Intelligent New Energy Vehicle and the Hunan Collaborative Innovation Center of Green Automobiles. G.-L.H. acknowledges support from NSF EFRI under Award No. 1641078.

[1] M. Konig, S. Wiedmann, C. Brune, A. Roth, H. Buhmann, L. W. Molenkamp, X. L. Qi, and S. C. Zhang, Science **318**, 766 (2007).
[2] B. A. Bernevig, T. L. Hughes, and S. C. Zhang, Science **314**, 1757 (2006).
[3] M. Z. Hasan and C. L. Kane, Rev. Mod. Phys. **82**, 3045 (2010).
[4] D. Hsieh, D. Qian, L. Wray, Y. Xia, Y. S. Hor, R. J. Cava, and M. Z. Hasan, Nature (London) **452**, 970 (2008).
[5] L. Lu, J. D. Joannopoulos, and M. Soljaclc, Nat. Photonics **8**, 821 (2014).
[6] F. D. M. Haldane and S. Raghu, Phys. Rev. Lett. **100**, 013904 (2008).
[7] S. Raghu and F. D. M. Haldane, Phys. Rev. A **78**, 033834 (2008).
[8] Z. Wang, Y. D. Chong, J. D. Joannopoulos, and M. Soljacic, Phys. Rev. Lett. **100**, 013905 (2008).

[9] Z. Wang, Y. D. Chong, J. D. Joannopoulos, and M. Soljacic, Nature (London) **461**, 772 (2009).

[10] Y. Poo, R. X. Wu, Z. F. Lin, Y. Yang, and C. T. Chan, Phys. Rev. Lett. **106**, 093903 (2011).

[11] K. J. Fang, Z. F. Yu, and S. H. Fan, Phys. Rev. B **84**, 075477 (2011).

[12] K. J. Fang, Z. F. Yu, and S. H. Fan, Nat. Photonics **6**, 782 (2012).

[13] R. O. Umucalilar and I. Carusotto, Phys. Rev. A **84**, 043804 (2011).

[14] M. Hafezi, E. A. Demler, M. D. Lukin, and J. M. Taylor, Nat. Phys. **7**, 907 (2011).

[15] M. Hafezi, S. Mittal, J. Fan, A. Migdall, and J. M. Taylor, Nat. Photonics **7**, 1001 (2013).

[16] A. B. Khanikaev, S. H. Mousavi, W. K. Tse, M. Kargarian, A. H. MacDonald, and G. Shvets, Nat. Mater. **12**, 233 (2013).

[17] M. C. Rechtsman, J. M. Zeuner, Y. Plotnik, Y. Lumer, D. Podolsky, F. Dreisow, S. Nolte, M. Segev, and A. Szameit, Nature (London) **496**, 196 (2013).

[18] L. Lu, L. Fu, J. D. Joannopoulos, and M. Soljacic, Nat. Photonics **7**, 294 (2013).

[19] W.-J. Chen, S.-J. Jiang, X.-D. Chen, B. Zhu, L. Zhou, J.-W. Dong, and C. T. Chan, Nat. Commun. **5**, 5782 (2014).

[20] W. Gao, M. Lawrence, B. Yang, F. Liu, F. Fang, B. Béri, J. Li, and S. Zhang, Phys. Rev. Lett. **114**, 037402 (2015).

[21] L.-H. Wu and X. Hu, Phys. Rev. Lett. **114**, 223901 (2015).

[22] L. Lu, C. Fang, L. Fu, S. G. Johnson, J. D. Joannopoulos, and M. Soljačić, Nat. Phys. **12**, 337 (2016).

[23] D. Leykam, M. C. Rechtsman, and Y. D. Chong, Phys. Rev. Lett. **117**, 013902 (2016).

[24] W.-J. Chen, M. Xiao, and C. T. Chan, Nat. Commun. **7**, 13038 (2016).

[25] K. J. Fang and S. H. Fan, Phys. Rev. Lett. **111**, 203901 (2013).

[26] D. L. Sounas, C. Caloz, and A. Alu, Nat. Commun. **4**, 2407 (2013).

[27] N. A. Estep, D. L. Sounas, J. Soric, and A. Alu, Nat. Phys. **10**, 923 (2014).

[28] L. D. Tzuang, K. Fang, P. Nussenzveig, S. H. Fan, and M. Lipson, Nat. Photonics **8**, 701 (2014).

[29] M. A. Bandres, M. C. Rechtsman, and M. Segev, Phys. Rev. X **6**, 011016 (2016).

[30] X. Cheng, C. Jouvaud, X. Ni, S. H. Mousavi, A. Z. Genack, and A. B. Khanikaev, Nat. Mater. **15**, 542 (2016).

[31] T. Ma, A. B. Khanikaev, S. H. Mousavi, and G. Shvets, Phys. Rev. Lett. **114**, 127401 (2015).

[32] L. M. Nash, D. Kleckner, A. Read, V. Vitelli, A. M. Turner, and W. T. M. Irvine, Proc. Natl. Acad. Sci. USA **112**, 14495 (2015).

[33] P. Wang, L. Lu, and K. Bertoldi, Phys. Rev. Lett. **115**, 104302 (2015).

[34] Z.-Y. Ong and C. H. Lee, Phys. Rev. B **94**, 134203 (2016).

[35] R. Süsstrunk and S. D. Huber, Proc. Natl. Acad. Sci. USA **113**, E4767 (2016).

[36] H. Nassar, H. Chen, A. N. Norris, M. R. Haberman, and G. L. Huang, Proc. R. Soc. London, Ser. A **473**, 20170188 (2017).

[37] H. Nassar, X. C. Xu, A. N. Norris, and G. L. Huang, J. Mech. Phys. Solids **101**, 10 (2017).

[38] R. Fleury, D. L. Sounas, C. F. Sieck, M. R. Haberman, and A. Alù, Science **343**, 516 (2014).

[39] A. B. Khanikaev, R. Fleury, S. H. Mousavi, and A. Alù, Nat. Commun. **6**, 8260 (2015).

[40] X. Ni, C. He, X. C. Sun, X. P. Liu, M. H. Lu, L. Feng, and Y. F. Chen, New J. Phys. **17**, 053016 (2015).

[41] Z. Yang, F. Gao, X. Shi, X. Lin, Z. Gao, Y. Chong, and B. Zhang, Phys. Rev. Lett. **114**, 114301 (2015).

[42] Z.-G. Chen and Y. Wu, Phys. Rev. Appl. **5**, 054021 (2016).

[43] R. Fleury, D. L. Sounas, and A. Alù, Phys. Rev. B **91**, 174306 (2015).

[44] R. Fleury, A. Khanikaev, and A. Alu, Nat. Commun. **7**, 11744 (2016).

[45] Y. G. Peng, C. Z. Qin, D. G. Zhao, Y. X. Shen, X. Y. Xu, M. Bao, H. Jia, and X. F. Zhu, Nat. Commun. **7**, 13368 (2016).

[46] C. He, Z. Li, X. Ni, X.-C. Sun, S.-Y. Yu, M.-H. Lu, X.-P. Liu, and Y.-F. Chen, Appl. Phys. Lett. **108**, 031904 (2016).

[47] Q. Wei, Y. Tian, S. Y. Zuo, Y. Cheng, and X. J. Liu, Phys. Rev. B **95**, 094305 (2017).

[48] Y. Li, Y. Wu, and J. Mei, Appl. Phys. Lett. **105**, 014107 (2014).

[49] S.-Y. Yu, Q. Wang, L.-Y. Zheng, C. He, X.-P. Liu, M.-H. Lu, and Y.-F. Chen, Appl. Phys. Lett. **106**, 151906 (2015).

[50] Y. Li and J. Mei, Opt. Express **23**, 12089 (2015).

[51] L. Xu, H. X. Wang, Y. D. Xu, H. Y. Chen, and J. H. Jiang, Opt. Express **24**, 18059 (2016).

[52] S. H. Kim, S. Kim, and C. S. Kee, Phys. Rev. B **94**, 085118 (2016).

[53] Z. G. Chen, X. Ni, Y. Wu, C. He, X. C. Sun, L. Y. Zheng, M. H. Lu, and Y. F. Chen, Sci. Rep. **4**, 4613 (2014).

[54] C. He, X. Ni, H. Ge, X.-C. Sun, Y.-B. Chen, M.-H. Lu, X.-P. Liu, L. Feng, and Y.-F. Chen, Nat. Phys. **12**, 1124 (2016).

[55] Z. W. Zhang, Q. Wei, Y. Cheng, T. Zhang, D. J. Wu, and X. J. Liu, Phys. Rev. Lett. **118**, 084303 (2017).

[56] J. Y. Lu, C. Y. Qiu, S. J. Xu, Y. T. Ye, M. Z. Ke, and Z. Y. Liu, Phys. Rev. B **89**, 134302 (2014).

[57] J. Mei, Y. Wu, C. T. Chan, and Z. Q. Zhang, Phys. Rev. B **86**, 035141 (2012).

[58] G. van Miert and C. M. Smith, Phys. Rev. B **93**, 035401 (2016).

[59] L. P. Ye, C. Y. Qiu, J. Y. Lu, X. H. Wen, Y. Y. Shen, M. Z. Ke, F. Zhang, and Z. Y. Liu, Phys. Rev. B **95**, 174106 (2017).

[60] J. Y. Lu, C. Y. Qiu, M. Z. Ke, and Z. Y. Liu, Phys. Rev. Lett. **116**, 093901 (2016).

[61] J. Y. Lu, C. Y. Qiu, L. P. Ye, X. Y. Fan, M. Z. Ke, F. Zhang, and Z. Y. Liu, Nat. Phys. **13**, 369 (2017).

[62] L. Feng *et al.*, Phys. Rev. B **73**, 193101 (2006).

[63] H. Q. Dai, T. T. Liu, J. R. Jiao, B. Z. Xia, and D. J. Yu, J. Appl. Phys. **121**, 135105 (2017).

[64] S. H. Mousavi, A. B. Khanikaev, and Z. Wang, Nat. Commun. **6**, 8682 (2015).

[65] See Supplemental Material at http://link.aps.org/supplemental/10.1103/PhysRevB.96.094106 for the band folding processes, the filling ratio dependent frequencies for the double Dirac cone, the angular-dependent frequencies for the four band edges at the Γ_2 point, band structures of phononic crystal with different rotating angles, simulated acoustic pressure field for the case with a zigzag interface and linear interfaces, stimulated acoustic pressure fields along an asteroid pathway, and an "HNU"-like pathway.

[66] C. He, X. L. Chen, M. H. Lu, X. F. Li, W. W. Wan, X. S. Qian, R. C. Yin, and Y. F. Chen, Appl. Phys. Lett. **96**, 111111 (2010).